Supporting Information

Mengge Zhang,[a]# Wenhu Zhang,[a]# Yawei Niu,[b] Xiao Tang,[a] Pin Lv,*[a, d] Jie Xu,[a] Xiaoyue Fa,[a] Chutong Zhang,[a] Liaokuo Gong,[c.d] Zhaolai Chen*[b] and Xiaobing Liu*[a, d]

[a] M. Zhang, W. Zhang, X. Tang, P. Lv, J. Xu, X. Fa, C. Zhang, X. Liu
Laboratory of High Pressure Physics and Material Science (HPPMS), Key Laboratory of Quantum Materials Under Extreme Conditions in Shandong Province, School of Physics and Physical Engineering, Qufu Normal University, Qufu, Shandong Province, 273165, China
*E-mail: lvpin@qfnu.edu.cn; xiaobing.phy@qfnu.edu.cn
[b] Y. Niu, Z. Chen
School of State Key Laboratory of Crystal Materials, and Institute of Crystal Materials, Shandong University, Jinan, 250100, China
*E-mail: zhaolaichen@sdu.edu.cn
[c] L. Gong
School of Chemistry and Chemical Engineering, Qufu Normal University, Qufu, Shandong Province, 273165, China
[d] P. Lv, L, Gong, X. Liu
Advanced Research Institute of Multidisciplinary Sciences, Qufu Normal University, Qufu, Shandong Province, 273165, China
# M. Zhang, W. Zhang contributed equally to this work
* Corresponding authors

Materials and Methods

Synthesis of single crystal samples of (4PPY)PbI_3 and (4,4'-TMDP)Pb_2I_6: We used acid precipitation method to synthesize (4PPY)PbI_3 single crystal samples. 0.5 mmol of lead(II) acetate trihydrate and 0.5 mmol of 4-(3-Phenylpropyl)pyridine were dissolved in a mixture of 5 ml of hydroiodic acid and 1 ml of hypophosphorous acid. The mixed solution was heated at 120 °C while being stirred continuously in an oil bath. The solution was stirred for 2 h until entirely dissolved, when it turned into clear and transparent yellow solution, stopped heating and stirring, and cool to 30 °C. Yellow, transparent, needle-like crystals precipitated during cooling. We synthesized (4,4'-TMDP)Pb_2I_6 single crystal samples using the acid precipitation method. 5 mmol of lead(II) acetate and 5 mmol of 4,4'-trimethylenedipyridine were dissolved in a mixture of 150 ml of hydroiodic acid and 20 ml of hypophosphorous acid. The mixed solution was heated at 120 °C and continuously stirred in an oil bath. Once the solution became clear and transparent, heating stopped and stirring to cool down naturally to room temperature, and the cooling process lasted for 12 h. Yellow, transparent, needle-like crystals precipitated during cooling.

Sample Preparation for High Pressure experiments: High-pressure experiments were conducted using symmetrical diamond anvil cells (DAC) equipped with type-IIa diamond anvils (400 µm culets) to reach pressures of 25-30 GPa. A T301 steel gasket, 1 mm thick and pre-indented to a thickness of 25-30 µm, was employed. A ruby ball approximately 10 µm in diameter served for pressure calibration within the 250 µm chamber, while liquid water was utilized as the pressure transfer medium.

In-situ High-pressure Characterizations and Measurements: The crystal structure of the synthesized samples was analyzed using a powder X-ray diffractometer with Cu-Kα radiation (λ = 1.5405 Å, Rigaku Smartlab SE, Japan). Raman spectroscopy was performed on a high-resolution spectrometer (Horiba, Lab-RAM HR Revolution) over the range of 50-3500 cm^{-1}, utilizing a 633 nm excitation laser with a 600 g/mm grating. Photoluminescence (PL) and absorption spectra were recorded with a custom-built system, employing a UV laser at 360 nm for PL excitation, with a consistent laser power density of 11 µW across all measurements. The absorption spectra were obtained using a xenon lamp (250 W, FLY-LX) as the light source, coupled with a fiber optic spectrometer (FX2000). The bandgap was determined by extrapolating the linear portion of the α^2 versus hv curve, where α represents the absorption coefficient, h is Planck's constant, and v is the photon frequency.

First-principles calculations: First-principles calculations for structure optimization and density of states were conducted using density-functional theory (DFT), specifically employing the Perdew-Burke-Ernzerhof (PBE) generalized gradient approximation (GGA) as implemented in the Vienna Ab initio Simulation Package (VASP). A plane wave cut-off energy of 600 eV was applied, along with k-point meshes featuring a spacing of 0.15 $Å^{-1}$, to ensure adequate convergence of the total energy, which was achieved with a precision of 10^{-5} eV. Atomic positions were fully relaxed until the forces acting on each atom fell below 10^{-3} eV $Å^{-1}$

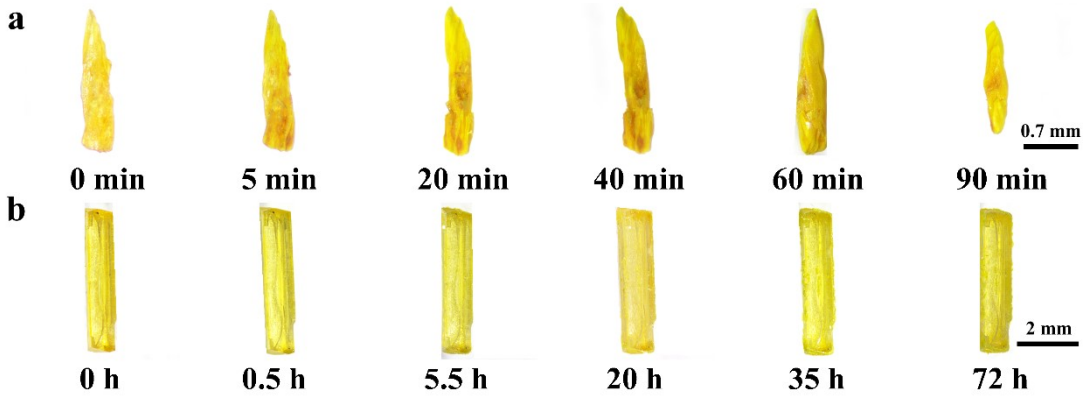

Figure S1. Water stability test of a) (4PPY)PbI_3 and b) (4,4'-TMDP)Pb_2I_6. One-dimensional single crystal samples were placed on a single concave carrier fragment dripping with water. The changes of samples' morphology with time increasing were observed. We found that the edge of (4PPY)PbI_3 began to passivate after 20 minutes, and the sample size decreased significantly after 90 minutes. The morphology of (4,4'-TMDP)Pb_2I_6 did not change significantly within 20 hours and could remain stable. After that, it was observed that the sample began to dissolve slightly.

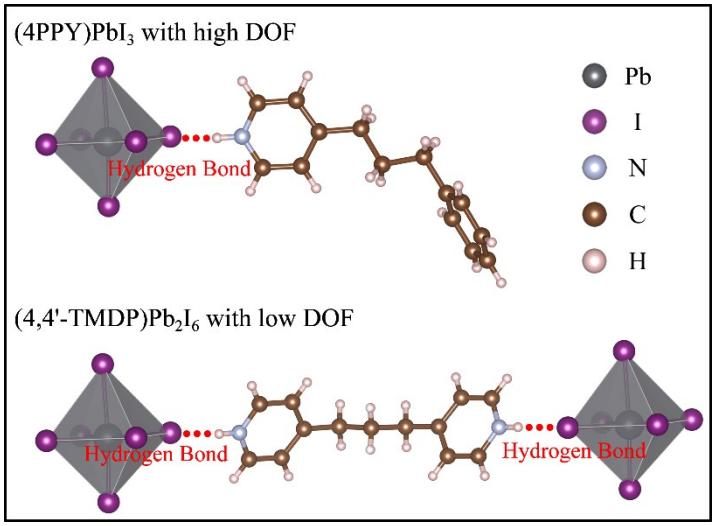

Figure S2. The structure diagram of (4PPY)PbI_3 with high DOF and (4,4'-TMDP)Pb_2I_6 with low DOF.

For (4PPY)PbI_3, the N-H bond in the pyridine ring at one end interacts with the inorganic framework through hydrogen bonding, while the benzene ring at the opposite end creates a van der Waals gap. This unique configuration facilitates the free rotation of the long chain, promoting structural cohesion and resulting in a high DOF. While for (4,4'-TMDP)Pb_2I_6 with low DOF, the N-H bonds in the pyridine rings at both ends of the organic cations interact with the inorganic framework, aligning the long chains in an orderly fashion with reduced DOF.

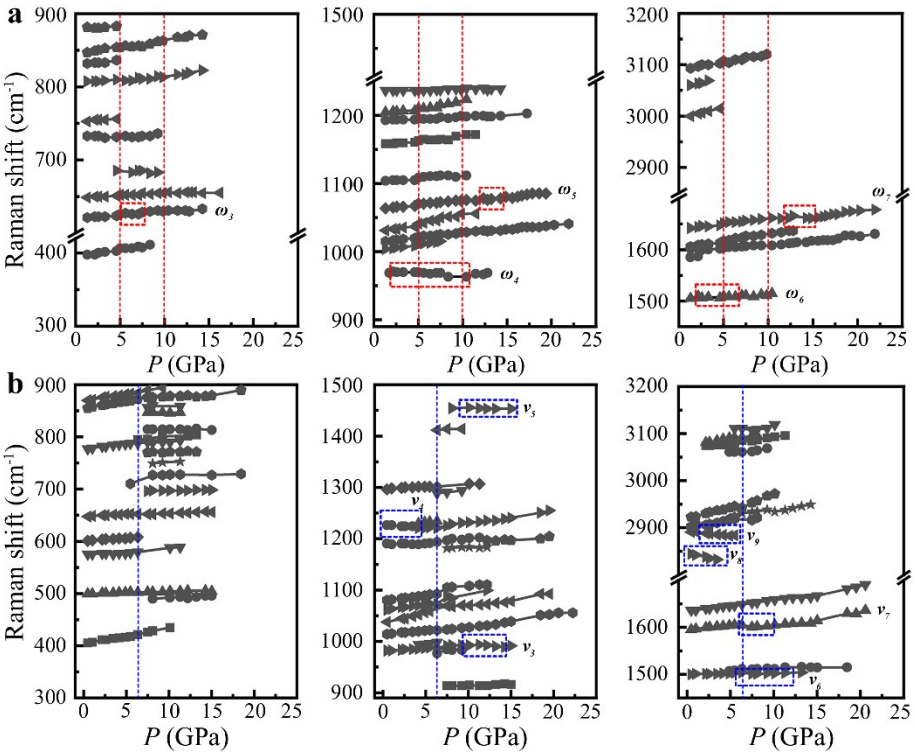

Figure S3. The raman shift of a) (4PPY)PbI_3 and b) (4,4'-TMDP)Pb_2I_6 in the range of 300-3200 cm^{-1}, respectively. The dashed boxes indicate the pressure ranges where softening of the vibrational modes occurs, as illustrated in Figures 2c and 2f of the main text. The pressure interval for (4PPY)PbI_3 is categorized into three stages based on the emergence and disappearance of Raman peaks: I (0-5 GPa), II (5-10 GPa), and III (10-25 GPa). At pressures of 5 GPa and 10 GPa, several new vibrational modes emerge while others vanish. In contrast, the pressure interval for (4,4'-TMDP)Pb_2I_6 is divided into two stages: I (0-6 GPa) and II (6-30 GPa). At 6 GPa, similar to (4PPY)PbI_3, new vibrational modes appear while others disappear.

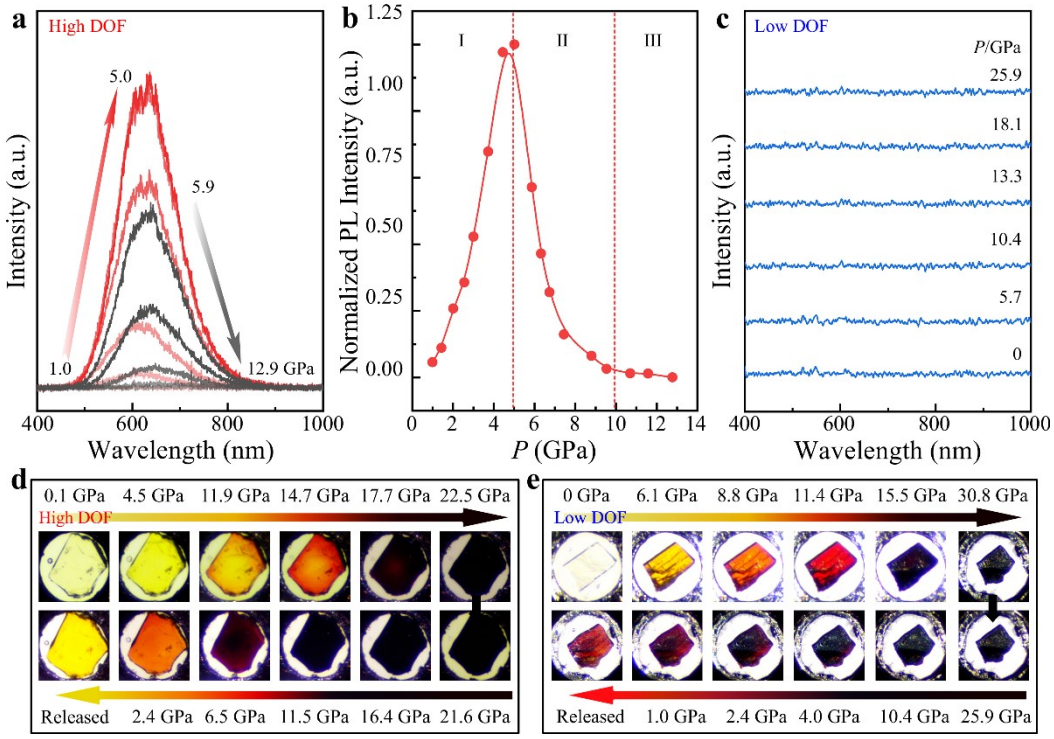

Figure S4. a) PL intensity of (4PPY)PbI_3 and c) (4,4'-TMDP)Pb_2I_6 under compression in a DAC chamber with silicone oil as pressure transmitting medium. b) Normalized PL intensity of (4PPY)PbI_3 with pressure increasing. Optical images of pressure-induced color changes of d) (4PPY)PbI_3 and e) (4,4'-TMDP)Pb_2I_6 under compression and decompression with silicone oi as pressure transmitting medium.

Table S1. Crystal data for (4PPY)PbI_3 at 298 K.

Temperature	298 K
Empirical formula	$C_{14}H_{16}I_3NPb$
Formula weight	786.17
Crystal system	triclinic
Space group	*P*-1
a (Å)	9.1943(5)
b (Å)	16.2348(8)
c (Å)	51.590(3)
α (°)	99.031(2)
β (°)	93.813(3)
γ (°)	90.100(2)
Volume (Å)	7587.9(7)
Z	16
*ρ*calc (g/cm^3)	2.753
μ (mm^{-1})	13.765
F(000)	5568.0
Radiation (Mo K*α*)	0.71073
2θ range for date collection (°)	3.762 to 55.016
Reflections collected	72385
Independent reflections	34483 [R(int) = 0.0551]
Date/restraints/parameters	34483/0/1376
Goodness-of-fit on F^2	1.035
Final R indexes [I>=2*σ*(I)]	R_1 = 0.0486, wR_2 = 0.1080
Final R indexes [all date]	R_1 = 0.0784, wR_2 = 0.1231

Table S2. Crystal data for (4,4'-TMDP)Pb_2I_6 at 298 K.

Temperature	298 K
Empirical formula	$C_{13}H_{16}I_6N_2Pb_2$
Formula weight	1376.06
Crystal system	monoclinic
Space group	*C*2/*c*
a (Å)	24.8636(11)
b (Å)	4.6503(2)
c (Å)	23.0345(10)
α (°)	90
β (°)	105.197(2)
γ (°)	90
Volume (Å)	2570.2(2)
Z	4
*ρ*calc (g/cm^3)	3.556
μ (mm^{-1})	20.291
F(000)	2360.0
Radiation (Mo K*α*)	0.71073
2θ range for date collection (°)	5.612 to 61.396
Reflections collected	20663
Independent reflections	3980 [R(int) = 0.0545]
Date/restraints/parameters	3980/0/106
Goodness-of-fit on F^2	1.051
Final R indexes [I>=2*σ*(I)]	R_1 = 0.0269, wR_2 = 0.0466
Final R indexes [all date]	R_1 = 0.0485, wR_2 = 0.0526

Table S3. Raman vibrational modes of (4PPY)PbI_3.

Peak position (cm^{-1})	Mode	Vibrational assignment	Reference
57.9	ω_1	Pb-I-Pb bending	1
63.1	ω_2	Pb-I-Pb bending	1
112.5	ω_3	Pb-I stretching	2
621.2	ω_4	in-plane bending of the pyridine ring	3
968.6	ω_5	in-plane bending of the pyridine ring	3
1063.5	ω_6	pyridine ring stretching and C-H bending	3
1505.2	ω_7	C–H/N–H in-plane wagging	4
1642.2	ω_8	C-C/N-H stretching	4

Table S4. Raman vibrational modes of (4,4'-TMDP)Pb_2I_6.

Peak position (cm^{-1})	Mode	Vibrational assignment	Reference
63.7	v_1	Pb-I-Pb bending	1
119.0	v_2	Pb-I stretching	2
981.2	v_3	in-plane bending of the pyridine ring	3
1227.6	v_4	pyridine ring stretching and C-H bending	3, 5
1454.4	v_5	pyridine ring stretching and C-H bending	3
1502.0	v_6	C–H/N–H in-plane wagging	4
1594.4	v_7	C-C/N–H stretching	2, 5

2847.1	v_8	C-H bending	5, 6
2891.6	v_9	C-H bending	5, 6

Table S5. Summary of the emission range of pressure-induced emission (PIE) low-dimensional metal halides perovskites.

Chemical formula	Dimension	PIE pressure (GPa)	PIE range (nm)	Reference
Cs_4PbBr_6	0	3.3	400-850	7
Cs_4PbBr_6 NCs	0	3.0	350-880	8
$Cs_3Sb_2Br_9$ QDs	0	0.8	450-800	9
Cy_4BiBr_7	0	0.5	400-520	10
$(bmpy)_6Pb_3Br_{12}$	0	1.6	410-830	11
$C_4N_2H_{14}SnBr_4$	1	2.1	500-850	12
$(4PPY)PbI_3$	1	1.1	450-800	This work
$Cs_3Bi_2Cl_9$ NCs	2	0.8	400-800	13
$(BA)_4AgBiBr_8$	2	2.5	500-900	14

Table S6. Summary of quenched bandgap for metal halides perovskites.

Chemical formula	Dimension	Original bandgap (eV)	Quenched bandgap (eV)	Bandgap interception rate	Reference
$FAPbI_3$	3	1.489	1.447	3%	15

$Cs_2AgBiBr_6$	3	2.2	1.7	23%	16
$(BA)_2(MA)_2Pb_3I_{10}$	2	1.94	1.78	8%	17
$(AMP)PbCl_4$	1	3.89	3.66	6%	18
$(AMP)PbBr_4$	1	3.44	2.38	31%	18
$(4,4'\text{-}TMDP)Pb_2I_6$	1	2.90	1.90	34%	This work

REFERENCES:

1. K. Gjorgjevikj, M. Bukleski, S. Dimitrovska-Lazova and S. Aleksovska, J. Mol. Struct., 2023, 1293, 136236.
2. X. Yang, Y. Ni, Y. Zhang, Y. Wang, W. Yang, D. Luo, Y. Tu, Q. Gong, H. Yu and R. Zhu, ACS Energy Lett., 2021, 6, 2404-2412.
3. K. K. Zhuravlev, K. Traikov, Z. Dong, S. Xie, Y. Song and Z. Liu, Phys. Rev. B, 2010, 82, 064116.
4. Z. Yu, W. Yu, J. Xing, R. A. Ganeev, W. Xin, J. Cheng and C. Guo, ACS Photonics, 2018, 5, 1619-1627.
5. F. P. Ureña, M. F. Gómez, J. J. L. González and E. M. n. Torres, SPECTROCHIM ACTA A, 2003, 59, 2815-2839.
6. L. Zhang, Y. Bai, Z. Shang, Y. Zhang and Y. Mo, J. Raman Spectrosc, 2007, 38, 1106-1111.
7. V. Drushliak, K. J. Kapcia and M. Szafran´sk, J. Mater. Chem. C., 2024, 12, 4360.
8. Z. Ma, Z. Liu, S. Lu, L. Wang, X. Feng, D. Yang, K. Wang, G. Xiao, L. Zhang, S. A. T. Redfern and B. Zou, Nat. Commun., 2018, 9, 4506.
9. F. Wang, J. Yang, T. Geng, P. Lv, D. Zhao, Y. Li, Q. Dong, G. Xiao and B. Zou, Mater. Res. Lett., 2024, 12, 500-506.
10. ME. Sun, T. Geng, X. Yong, S. Lu, G. Xiao, J. Cai, B. Zou and SQ. Zang, Adv. Sci., 2021, 8, 2004853.
11. M. Chen, S. Guo, K. Bu, S. Lee, H. Luo, Y. Wang, B. Liu, Z. Yan, H. Dong, W. Yang, B. Ma and X. Lü, Matter Radiat. Extremes, 2021, 6, 058401.
12. Y. Shi, Z. Ma, D. Zhao, Y. Chen, Y. Cao, K. Wang, G. Xiao and B. Zou, J. Am. Chem. Soc., 2019, 141, 6504-6508.
13. T. Geng, Y. Shi, Z. Liu, D. Zhao, Z. Ma, K. Wang, Q. Dong, G. Xiao and B. Zou, J. Phys. Chem. Lett., 2022, 13, 11837-11843.
14. Y. Fang, L. Zhang, L. Wu, J. Yan, Y. Lin, K. Wang, W. L. Mao and B. Zou, Angew. Chem. Int. Ed., 2019, 58, 15249-152523.
15. G. Liu, L. Kong, J. Gong, W. Yang, H.-k. Mao, Q. Hu, Z. Liu, R. D. Schaller, D. Zhang and T. Xu, Adv. Funct. Mater., 2017, 27, 1604208.
16. Q. Li, Y. Wang, W. Pan, W. Yang, B. Zou, J. Tang and Z. Quan, Angew. Chem. Int. Ed., 2017, 56, 15969-15973.
17. G. Liu, J. Gong, L. Kong, R. D. Schaller, Q. Hu, Z. Liu, S. Yan, W. Yang, C. C. Stoumpos, M. G. Kanatzidis, H.-k. Mao and T. Xu, PNAS., 2018, 115, 8076-8081.
18. X. Wu, Y. Sun, L. Wang, Y. Huang, J. Wang, Y. Yuan, U. Shahzadi, R. Fu, K. Wang and H. Guo, Adv. Opt. Mater., 2025, 13, 2402136.